

# Single Electron Charge Sensitivity of Liquid-Gated Carbon Nanotube Transistors

Tal Sharf,<sup>†</sup> Neng-Ping Wang,<sup>‡</sup> Joshua W. Kevek,<sup>§</sup> Morgan A. Brown,<sup>†</sup> Heather Wilson,<sup>†</sup> Stefan Heinze,<sup>||</sup> and Ethan D. Minot<sup>\*,†</sup>

<sup>†</sup>Department of Physics, Oregon State University, Corvallis, Oregon 97331-6507, United States

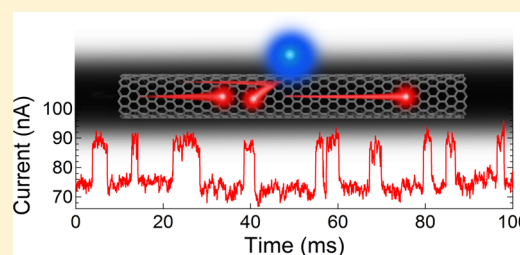
<sup>‡</sup>Science Faculty, Ningbo University, Ningbo 315211, People's Republic of China

<sup>§</sup>Laboratory of Atomic and Solid-State Physics, Cornell University, Ithaca, New York 14883, United States

<sup>||</sup>Institute of Theoretical Physics and Astrophysics, University of Kiel, Kiel D-24098, Germany

## Supporting Information

**ABSTRACT:** Random telegraph signals corresponding to activated charge traps were observed with liquid-gated CNT FETs. The high signal-to-noise ratio that we observe demonstrates that single electron charge sensing is possible with CNT FETs in liquids at room temperature. We have characterized the gate-voltage dependence of the random telegraph signals and compared to theoretical predictions. The gate-voltage dependence clearly identifies the sign of the activated trapped charge.



**KEYWORDS:** Carbon nanotube, low-frequency noise, random telegraph signals, single charge, charge traps, liquid-gate

The pursuit to miniaturize transistor technologies down to nanometer scale dimensions has been driven by a demand for low power, high performance, and high sensitivity electronic applications. Carbon nanotube field-effect transistors (CNT FETs) are promising candidates to satisfy these demands. Technological advances in device designs have paved the way for scalable CNT based digital switches,<sup>1,2</sup> which combined with recent advances in CNT synthesis offer an alternate route to silicon based technologies.<sup>3,4</sup> Additionally, the remarkable sensitivity of CNT FET sensors has recently been used to measure single-molecule processes such as DNA hybridization,<sup>5</sup> single chemical reactions,<sup>6</sup> and single enzyme activity.<sup>7</sup> These measurements are sensitive to molecules carrying a handful of charges, suggesting that CNTs can reach single electron charge sensitivity in liquids at room temperature.

The high sensitivity of CNT FETs comes at the price of ever-present charge noise. Charge noise is typically manifested as stochastic current fluctuations with a power spectral density that scales inversely with frequency ( $f$ ). In typical CNT devices this  $1/f$  noise spectrum is attributed to a large number of charge traps near the CNT channel. The charge noise model developed by Tersoff assumes a capacitive coupling between these fluctuating charge traps and the CNT channel.<sup>8</sup> Tersoff's model has been experimentally verified for both liquid-gated CNT FETs and graphene FETs.<sup>9,10</sup>

In small devices, such as CNT FETs, a single charge trap can have a disproportionately large influence, leading to the observation of a random telegraph signal (RTS) when measuring conductance vs time.<sup>11–18</sup> For example, one charge trap might be located a few Angstroms from the CNT channel, while all other traps are more distant. Random telegraph signals

in CNT FETs have been studied extensively at low temperature,<sup>13–18</sup> and two studies have reported RTS at room temperature, demonstrating that single charge sensitivity is possible in air and vacuum.<sup>11,12</sup> This previous work has also verified the gate-dependent capture time and emission time can be understood in a framework developed for RTS in metal-oxide-semiconductor FET devices.<sup>19</sup>

In this work, we explore RTS at room temperature in electrolyte-gated CNT FETs. The electrolyte gate ensures almost perfect coupling between the gate voltage and the Fermi level in the CNT, allowing clear comparisons between experiment and theory. The elevated temperature ensures that charge hopping between the CNT and the trap state occurs over a wide range of gate voltages. While previous experiments have characterized RTS switching dynamics (capture times and emission times), we focus on the gate-dependent amplitude of the RTS signal. We compare our results to non-equilibrium Green's function (NEGF) calculations of scattering from a Coulomb potential created by a point charge. Our measurements confirm theoretical predictions for the gate voltage dependence of the RTS amplitude.<sup>20</sup> Our results are a key test of the NEGF modeling approach and open a path to rational design of single molecule electronic detectors.

**Results. Device Architecture.** Carbon nanotube devices were fabricated using standard photolithography and metal

**Received:** October 24, 2013

**Revised:** July 28, 2014

deposition techniques (see Methods). Figure 1a shows a schematic diagram of the device geometry utilized for

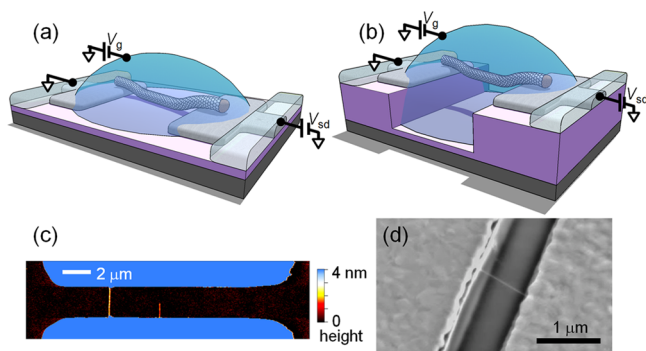


**Figure 1.** (a) Schematic diagram of a single surface-bound CNT device operating in liquid. (b) Diagram of a suspended CNT device. (c) Surface topography map of a single surface-bound CNT device measured by AFM. (d) Scanning electron micrograph of a single suspended CNT device.

performing measurements on surface-bound CNT FETs while operating in liquid environments. The CNTs were grown as a final processing step using “fast heat” chemical vapor deposition, which yields ultraclean devices.<sup>21</sup> Devices with single CNTs were verified by AFM characterization as shown in Figure 1c. Semiconducting CNT devices were chosen for electronic measurements with a diameter range of 1–2 nm. For measurements on suspended CNT devices, a reactive ion etch was used to remove the SiO<sub>2</sub>/Si<sub>3</sub>N<sub>4</sub> between a 1 μm source-drain electrode gap, producing an ideal geometry to grow ultraclean suspended CNT devices (Figure 1b,d).<sup>22</sup> A home-built laminar flow cell was used to interface the CNT devices with 10 mM phosphate buffer (PB). The Debye screening length of this electrolyte solution is ~3 nm. The solution potential was set by a Ag/AgCl reference electrode<sup>23</sup> or on-chip Pt electrode. Electrochemical currents between the liquid and the CNT device never exceeded 100 pA.

**Substrate Induced RTS Noise in CNT FETs.** Figure 2a shows current versus time,  $I(t)$ , measured from a single surface-bound

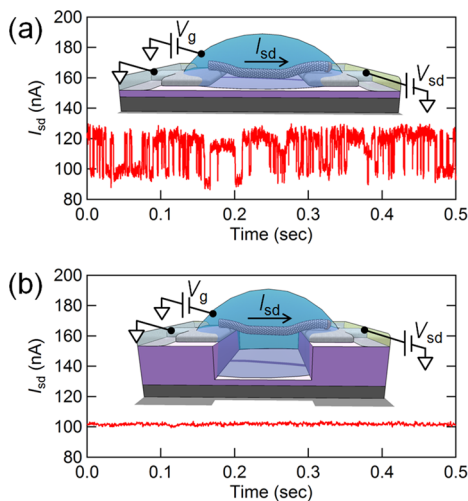


**Figure 2.** (a) Two-level current noise exhibited by a single surface-bound CNT device operating in 10 mM PB. (b) Current measured through a suspended device operating in the same conditions as (a).

CNT operating in a solution of 10 mM PB. Switching events occur between two well-defined levels of current, which are defined by a high-current state  $I_{\text{high}}$  and a low-current state  $I_{\text{low}}$ . Random telegraph signals such as Figure 2a were observed in 8 out of 24 surface-bound devices (see Supporting Information Part A for surface and charge trap spatial overlap probabilities). The other 16 surface-bound devices exhibited fluctuating  $I(t)$  about a single current level. The power spectral density of these  $I(t)$  fluctuations exhibited a  $1/f$  spectrum as previously reported by Mannik et al.<sup>9</sup> Figure 2b shows an equivalent measurement performed on an ultraclean suspended device in similar conditions. We measured a total of 16 suspended CNTs and none showed RTS. For these suspended CNTs, the power spectral density of  $I(t)$  fluctuations was also significantly less.<sup>22</sup>

On the basis of the comparison of surface-bound and suspended CNTs (Figure 2), we conclude that the dielectric substrate is responsible for the observed RTS. When the chemical potential for electrons in the CNT coincides with the energy level of trap state, the occupancy of the trap can fluctuate. Following previous work, we attribute  $I_{\text{low}}$  and  $I_{\text{high}}$  to the fluctuating occupancy of such a trap.

**Gate-Dependence of Trap Occupation.** We first examine the relative probability of finding the device in the  $I_{\text{high}}$  state versus the  $I_{\text{low}}$  state. Figure 3 shows RTS measured from a surface-bound CNT at a variety of gate voltages,  $V_g$ . The  $I(V_g)$  characteristic of the device is shown in Figure 3a. At  $V_g < \sim -0.3$  V, the CNT is p-doped and has relatively high conductance. For  $V_g > \sim -0.3$  V, the conductance begins to follow an exponential decay (see inset of Figure 3a), indicative of the subthreshold regime where the Fermi level enters the bandgap. Figure 3b shows time traces,  $I(t)$ , obtained at different values of  $V_g$ . The time-averaged current drops as  $V_g$  is increased from  $-0.7$  to  $-0.2$  V. At  $V_g = -0.7$  V, the high-conductance RTS state is favored. At  $V_g = -0.35$  V, the low-conductance RTS state is favored. Following the interpretation of Ralls et al.,<sup>19</sup> we conclude that a negative scattering center turns on by electron capture; i.e., at negative gate voltages the trap state is neutral, at positive gate voltages, an electron spills out of the CNT into the trap state, and at intermediate gate voltages, the trap fluctuates between filled and empty (see Supporting Information Part B).

Two out of 8 devices showed gate-dependent trap occupation that was consistent with electron capture by a neutral trap state. In other devices, the liquid gate voltage had no effect on emission and capture times. A possible explanation for unperturbed emission and capture times is an extreme proximity between the trap and the CNT. If the capacitive coupling between the trap and the CNT is extremely strong, the liquid gate voltage will not change the relative energy difference.

**Doping Effect versus Mobility Effect.** When a trap state captures a charge, both the doping level and the effective mobility of the CNT are affected. NEGF simulations give insight into distinguishing these two effects. A distant charge will cause a smooth variation in potential and effectively change the doping level in the CNT. If the charge is more than ~3 nm away from the CNT, NEGF simulations predict that the change in current is simply proportional  $dI_{\text{sd}}/dV_g$ .<sup>20</sup> Experiments that measure conductance fluctuations in CNT FETs (the collective result of many charge traps) support this model.<sup>9,22</sup> In contrast, when the charge is closer than ~3 nm, NEGF simulations predict that electron scattering becomes significant and the change in current is not simply proportional to  $dI_{\text{sd}}/dV_g$ .

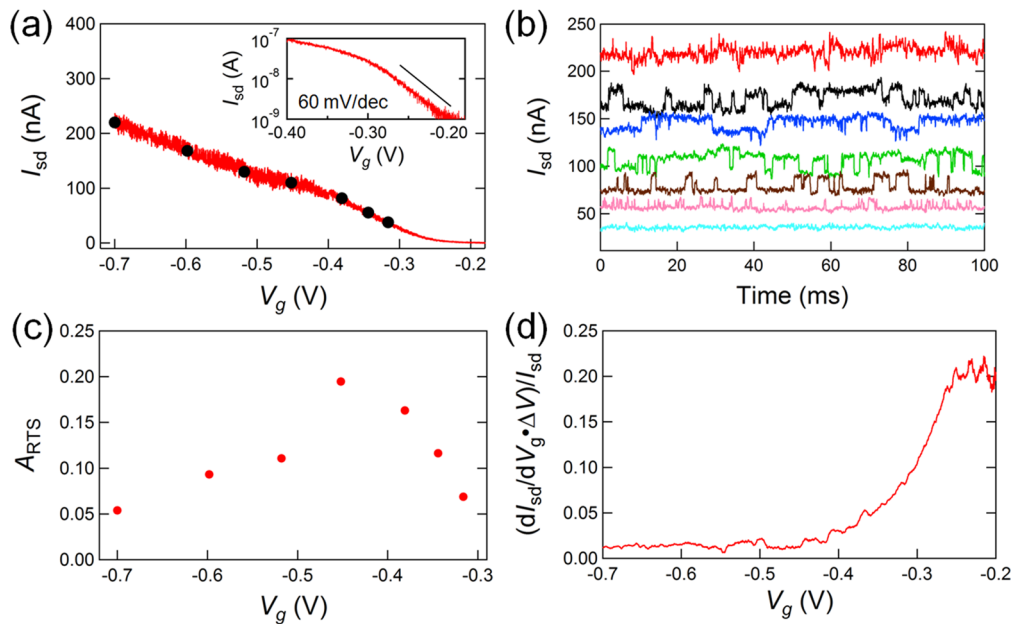


**Figure 3.** (a) Transistor curve of a surface-bound CNT FET exhibiting RTS current noise in 10 mM PB. The solid circles show where  $I_{sd}(t)$  data was collected. The inset shows the exponential subthreshold regime. (b) Current measured at fixed values of  $V_g$  shown as solid circles in (a). (c) Fractional change in current ( $A_{RTS}$ ) plotted as a function of gate voltage. (d) Fractional change in current predicted by doping mechanism for fixed jump in potential of  $\Delta V = 5$  mV.

To determine whether our RTS measurements can be described by doping, we plot the prediction for  $A_{RTS}$  ( $A_{RTS} = (I_{high} - I_{low})/I_{high}$ ) caused by a distant charge trap (Figure 3d). The slope of the transistor curve,  $dI_{sd}/dV_g$ , has been multiplied by a fitting parameter, 5 mV, and divided by  $I_{sd}$ , yielding a peak  $A_{RTS} = 0.2$ . The maximal value of  $A_{RTS}$  occurs in the subthreshold and stays constant throughout the subthreshold. In contrast, our measured values of  $A_{RTS}$  peak in the on-state, before the subthreshold, and decay in the subthreshold (Figure 3c). We carried out detailed  $A_{RTS}(V_g)$  measurements on 3 other devices that exhibited RTS current noise and observed similar trends. We conclude that carrier scattering must be considered to describe the measured RTS.

**Theoretical Modeling of RTS Amplitude.** Wang et al. previously calculated  $A_{RTS}$  for a ballistic CNT FETs interacting with a fluctuating single charge (either positive or negative).<sup>20</sup> We first discuss the qualitative conclusions from these simulations. For a positive charge trap interacting with a p-type device,  $A_{RTS}(V_g)$  increases monotonically as  $V_g$  is tuned from the p-doping to the subthreshold. For a negative charge trap, there is a peak in  $A_{RTS}(V_g)$  when  $V_g$  is near the transition between p-doping and the subthreshold regime. On the basis of these qualitative results, we conclude that our measured  $A_{RTS}(V_g)$  is consistent with the coming and going of a negative charge near the CNT.

We have extended the previous work of Wang et al. to give a more quantitative understanding of our particular experimental system. Our new calculations take into account non-ohmic contacts between the CNT and the metal electrodes, inelastic scattering in the CNT and the liquid gate geometry. We begin with NEGF simulations of an ohmically contacted (13, 0) CNT (diameter 1.04 nm) with a channel length of 200 nm, surrounded by a dielectric of either  $\epsilon = 4$  or 10, a cylindrical gate of radius 16 nm, and a negative charge (or no charge) near the sidewall of the CNT (separation distance  $d = 0.5$  or 1.5 nm). The source-drain voltage is 50 mV and  $T = 300$  K.

Current is calculated at different gate voltages, both with and without the single electron charge next to the CNT.

First, the parameters used in the NEGF simulation should be consistent with the liquid gated environment. Free ions diffusing in the water lead to an electrostatic screening length of  $\sim 3$  nm, but the simulations only account for screening by free carriers in the CNT. However, the simulated free-carrier screening lengths were 3 nm and shorter when the CNT was p-doped (higher hole concentration at negative gate voltages leads to shorter screening lengths, see Supporting Information Part C); therefore, screening by free ions in the water can be neglected to first order. Similarly, electrolyte gating is not explicitly modeled. Instead, the model uses a perfect cylindrical gate (see Figure 4b inset), which allows us to obtain comparable turn-on characteristics to the experimental device. Lastly, the experimental geometry includes two dielectrics, water ( $\epsilon = 80$ ) and  $\text{SiO}_2$  ( $\epsilon = 4$ ), but the simulations are performed with a single dielectric constant. Since the charge trap is in the  $\text{SiO}_2$ , initial calculations were performed with  $\epsilon = 4$ . Additional calculations with a higher effective epsilon ( $\epsilon = 10$ ) yielded  $A_{RTS}$  values that were a factor 2 smaller. If the effective dielectric constant is indeed 10 or higher, the proximity of the charge trap to the CNT,  $d$ , must be reduced to obtain agreement between experiment/theory values of  $A_{RTS}$ . Our current experiments cannot resolve this uncertainty in  $\epsilon$  and  $d$ .

To translate the results of the NEGF simulations (ballistic transport, ohmic contacts) into predictions for a diffusive 1d system with non-ohmic contacts, we make use of the Landauer formalism for addition of incoherent barriers.<sup>24</sup> In a diffusive 1d system, the Coulomb barrier associated with a charge trap adds a fixed amount of resistance  $\Delta R$  to the overall system.  $\Delta R$  is independent of channel length and contact resistance (see Supporting Information Part D for more details). Results from the NEGF simulations allow us to approximate  $\Delta R$  by calculating  $\Delta R^{\text{sim}} = R_0^{\text{sim}} - R_Q^{\text{sim}}$ , where  $R_0^{\text{sim}}$  is the simulated

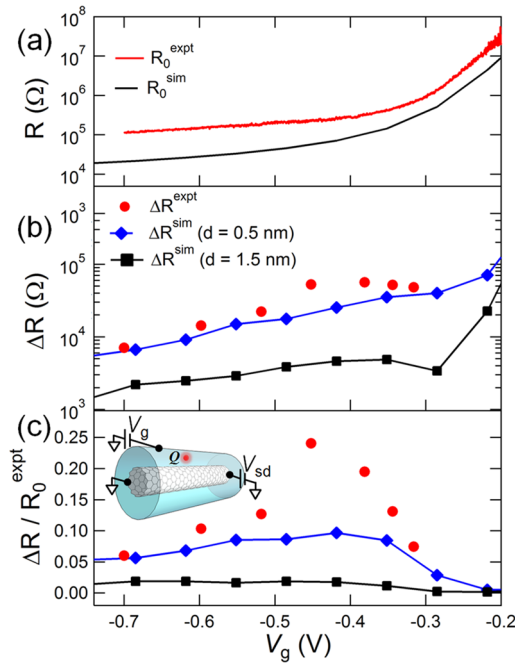


**Figure 4.** (a) Experimentally measured (red line) and NEGF simulated (black line) CNT resistance vs gate voltage. (b) Change in CNT resistance produced by RTS noise measured as a function gate voltage. Red circles are experimental results extracted from Figure 3b. Blue diamonds and black squares are NEGF predictions for scattering from a  $-1e$  charge placed a distance of 0.5 and 1.5 nm from the CNT sidewall, respectively. (c) Fractional resistance change where data from (b) is normalized by the baseline experimental resistance  $R_0^{\text{expt}}$ .

resistance with no charge, and  $R_Q^{\text{sim}}$  is the simulated resistance with a single charge. The simulated value  $\Delta R^{\text{sim}}$  includes interference effects caused by coherent multiple reflections. These effects are not present in the diffusive transport regime of our experiment, however, multiple reflections are a small correction in the situations studied here ( $A_{\text{RTS}} < 0.2$ ).

Figure 4a shows CNT device resistance plotted as a function of gate voltage  $R(V_g)$  for both experimental and NEGF simulated results. Our experimental devices have channel lengths of  $2 \mu\text{m}$  (see Figure 1c), which is  $\sim 3$  times larger than the phonon scattering length at room temperature.<sup>25</sup> Therefore, we expect the experimentally measured channel resistance to be 3 times more resistive than simulated NEGF data (channel resistance scales linearly with channel length in the diffusive limit<sup>25</sup>). This insight allows us to map the

experimental values of  $V_g$  onto the simulated values of  $V_g$  (differences between experimental and simulated  $V_g$  values are caused by factors such as the choice of liquid gate electrode and surface charges on the  $\text{SiO}_2$ ). The experimentally measured  $R(V_g)$  curve has been translated on the  $V_g$  axis so that the experimental subthreshold resistance is 3 times the subthreshold resistance of the simulation.

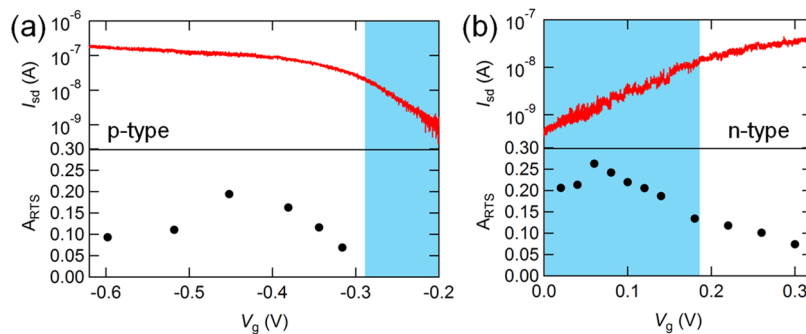
Figure 4b shows a comparison between  $\Delta R^{\text{sim}}$  and our experimental measurements. The  $\Delta R$  extracted from the RTS measurements varies from  $\sim 7 \text{ k}\Omega$  in the on-state to  $\sim 60 \text{ k}\Omega$  near the subthreshold regime (see Supporting Information Part E for  $\Delta R$  data from additional devices). The NEGF simulation results follow a similar trend. In Figure 4c, the  $\Delta R$  values have been divided by  $R_0^{\text{expt}}$  to show the fractional change in resistance. Both NEGF and experiments show that the fractional change is maximized as the device transitions from the on-state to subthreshold regimes.

Figure 4c highlights the influence of  $R_0^{\text{expt}}$  on RTS amplitude (note that  $\Delta R/R_0^{\text{expt}}$  equals  $A_{\text{RTS}}$  to within a correction factor of order unity;  $\Delta R/R_0^{\text{expt}} = A_{\text{RTS}} \cdot I_0/I_Q$ ). Large values of the baseline resistance  $R_0^{\text{expt}}$  will suppress  $A_{\text{RTS}}$ ; therefore, small  $R_0^{\text{expt}}$  is desirable for sensor applications. Previous work has shown  $R_0^{\text{expt}} = \rho L + R_c$ , when  $L > \lambda_{\text{in}}$ ;  $\rho$  is 1-d resistivity,  $R_c$  is contact resistance,  $L$  is the channel length and  $\lambda_{\text{in}}$  is the inelastic scattering length.<sup>25</sup> Optimal  $\Delta R/R_0^{\text{expt}}$  is expected when  $L \sim \lambda_{\text{in}}$ . Smaller  $L$  will not reduce  $R_0^{\text{expt}}$ , but smaller  $L$  will increase background noise ( $1/f$  noise), which scales as  $1/\sqrt{L}$ .<sup>9</sup>

**Dependence of RTS Amplitude on Carrier Type.** As a final test of our model, we have measured RTS in n-type CNT FETs. By changing the sign of charge carriers in the CNT channel, we expect a dramatic change in the gate-dependent scattering probability.

Figure 5 shows a side-by-side comparison of  $A_{\text{RTS}}$  in a p-type channel and an n-type channel (measurements from two different devices). The overall  $A_{\text{RTS}}$  magnitude is similar for the two devices, but the  $V_g$  dependence is strikingly different. As discussed above, all p-type devices in our study exhibited maximal  $A_{\text{RTS}}$  in the on-state. In contrast, the n-type device exhibits maximal  $A_{\text{RTS}}$  in the subthreshold (blue shaded region), with  $A_{\text{RTS}}$  remaining approximately constant within the subthreshold. We have observed this behavior for a total of 3 n-type devices.

The  $A_{\text{RTS}}(V_g)$  signature shown in Figure 5b is consistent with predictions for n-type carriers scattering from a negative charge trap.<sup>20</sup> For a trap charge and carrier charge of similar polarity,  $\Delta R^{\text{sim}}/R_0^{\text{sim}}$  reaches a maximal plateau in the subthreshold



**Figure 5.** Comparison between p-type and n-type CNT FETs that exhibit RTS. (a) Transistor curve for a p-type CNT circuit exhibiting RTS. Fractional change in current is shown in the lower graph. The subthreshold regime is shaded. (b) Transistor curve for an n-type CNT circuit exhibiting RTS. Fractional change in current is shown in the lower graph.

regime. The height of this plateau depends strongly on separation distance  $d$  and baseline resistance  $R_0^{\text{expt}}$ . The data shown in Figure 5b are consistent with a separation distance of a few nanometers. From the  $V_g$  dependence shown in Figure 5b, we conclude that the relative sign of the trap charge and carrier charge is indeed a critical parameter in determining  $A_{\text{RTS}}(V_g)$ .

**Conclusion.** In a room-temperature liquid environment, CNT FETs are capable of detecting signals generated by the coming and going of a single electron charge. The sign of the charge can be determined by measuring the gate-sensitivity of the RTS magnitude. We find good agreement between our measurements and the predictions of NEGF simulations, opening a path to optimizing the design of single-molecule bioelectronic sensors. Our measurements highlight the need to eliminate charge traps in the dielectrics of high-fidelity nanoelectronic devices, and confirm the exciting possibility of detecting single charges in room-temperature biological environments.

**Methods. Device Fabrication.** Metal electrodes (1 nm Ti, 50 nm Pt) were patterned on top of Si/SiO<sub>2</sub> (600  $\mu\text{m}/1 \mu\text{m}$ ) substrates or Si/SiO<sub>2</sub>/Si<sub>3</sub>N<sub>4</sub> (600  $\mu\text{m}/1 \mu\text{m}/100 \text{ nm}$ ). The metal electrode leads were passivated with 80 nm of e-gun deposited SiO<sub>2</sub> (excluding the source-drain electrode tips and probe contacts) to prevent Faradaic currents that occur during liquid gating. Catalyst islands (1 nm Ti, 40 nm SiO<sub>2</sub>, 1 nm Fe) of dimension 10  $\mu\text{m} \times 5 \mu\text{m}$  were patterned on the electrode tips a distance of 4  $\mu\text{m}$  from the edge of the source-drain electrode gap (2  $\mu\text{m}$ ). The devices were then diced into 2 cm chips. To prevent electrode degradation during the high temperature CNT growth process, it was crucial to limit chip exposure time to high temperatures. This was accomplished by implementing a quartz loading shuttle attached to a steel ball bearing and shuttling the chips in and out of the hot-zone of a 1 in. quartz tube furnace with an external magnet. The shuttle growth recipe is as follows: (1) Chips were first shuttle annealed in open air at 600 °C for 5 min. (2) The furnace was sealed and allowed to cool below 300 °C, purged for 2 min flowing the CNT growth gases (Argon bubbled methanol at 0.3 slm, Argon bubbled ethanol at 0.15 slm and H<sub>2</sub> at 0.45 slm), then flushed with Ar (1 slm) for 2 min to clear the growth gases from the chamber. (3) Chips were then shuttle annealed in H<sub>2</sub> (0.45 slm) for 1 min at 800 °C. (4) The furnace was ramped to 900 °C in H<sub>2</sub> (0.45 slm) and switched over to CNT growth gases, and chips were shuttled into the furnace for a 5 min CNT growth. The chips were cooled outside of the heat-zone under Argon (1 slm) until the heat-zone reached 200 °C, then furnace seals were opened to atmosphere. These growth parameters produced ~10% single CNT connections on surface-based devices with a 2  $\mu\text{m}$  source-drain electrode gap. To achieve similar yields on suspended devices with a 1  $\mu\text{m}$  source-drain channel gap, the growth parameters of step (4) were reduced to 800 °C.

**Electrical Measurements.** Single CNT devices were interfaced with a liquid environment (10 mM PB) using a home-built laminar flow cell. Current was measured through the devices using a Stanford Research Systems model SRS570 current preamplifier (sensitivity 100 nA/V, High bandwidth mode, no filters applied). The source-drain bias (25 mV) was supplied by the bias offset of the SRS570 current preamplifier, which was powered by an internal lead-acid battery. The liquid-gate voltage was applied to Ag/AgCl reference electrode (BASi RE-6) interfaced downstream of the flow cell using a Yokogawa

GS210 DC voltage source. Equivalent results were obtained using a lithographically defined on-chip Pt electrode of dimensions 200  $\mu\text{m} \times 1 \text{ mm}$ . The electrochemical currents between the liquid-gate and source-drain electrodes never exceeded 100 pA. To gain access to n-type regime of semiconducting CNT devices, a tungsten electrode was used to control the solution potential.

## ■ ASSOCIATED CONTENT

### 📄 Supporting Information

Estimation of the probability that a CNT lies directly on a charge trap, histograms showing the relative probability of high-current and low-current RTS states, plots of the screened Coulomb potential from NEGF simulations, theoretical framework for analyzing the resistance increase caused by a scattering, and measured values of  $\Delta R$  for additional devices. This material is available free of charge via the Internet at <http://pubs.acs.org>.

## ■ AUTHOR INFORMATION

### Corresponding Author

\*E-mail: [minote@science.oregonstate.edu](mailto:minote@science.oregonstate.edu).

### Notes

The authors declare no competing financial interest.

## ■ ACKNOWLEDGMENTS

We thank David Roundy and Alejandro Cortese for valuable discussions. This work was supported by the Oregon Nanoscience and Microtechnologies Institute (ONAMI) and the Human Frontiers Science Program (HFSP) under Grant No. RGY0058/2010. Sample fabrication was performed at the MaSC Facility at Oregon State University and the Cornell node of the National Nanofabrication Infrastructure Network, which is supported by the National Science Foundation (Grant ECS-0335765). N.-P.W. acknowledges financial support from The National Natural Science Foundation of China under Grant No. 61176081

## ■ REFERENCES

- (1) Shulaker, M. M.; Hills, G.; Patil, S.; Wei, H.; Chen, H.; Wong, H. S. P.; Mitra, S. *Nature* **2013**, *501* (7468), 526–530.
- (2) Franklin, A. D.; Koswatta, S. O.; Farmer, D. B.; Smith, J. T.; Gignac, L.; Breslin, C. M.; Han, S. J.; Tulevski, G. S.; Miyazoe, H.; Haensch, W.; Tersoff, J. *Nano Lett.* **2013**, *13* (6), 2490–2495.
- (3) Franklin, A. D. *Nature* **2013**, *498* (7455), 443–444.
- (4) Jin, S. H.; Dunham, S. N.; Song, J. Z.; Xie, X.; Kim, J. H.; Lu, C. F.; Islam, A.; Du, F.; Kim, J.; Felts, J.; Li, Y. H.; Xiong, F.; Wahab, M. A.; Menon, M.; Cho, E.; Grosse, K. L.; Lee, D. J.; Chung, H. U.; Pop, E.; Alam, M. A.; King, W. P.; Huang, Y. G.; Rogers, J. A. *Nat. Nanotechnol.* **2013**, *8* (5), 347–355.
- (5) Sorgenfrei, S.; Chiu, C. Y.; Gonzalez, R. L.; Yu, Y. J.; Kim, P.; Nuckolls, C.; Shepard, K. L. *Nat. Nanotechnol.* **2011**, *6* (2), 125–131.
- (6) Goldsmith, B. R.; Coroneus, J. G.; Kane, A. A.; Weiss, G. A.; Collins, P. G. *Nano Lett.* **2008**, *8* (1), 189–194.
- (7) Choi, Y. K.; Moody, I. S.; Sims, P. C.; Hunt, S. R.; Corso, B. L.; Perez, I.; Weiss, G. A.; Collins, P. G. *Science* **2012**, *335* (6066), 319–324.
- (8) Tersoff, J. *Nano Lett.* **2007**, *7* (1), 194–198.
- (9) Mannik, J.; Heller, I.; Janssens, A. M.; Lemay, S. G.; Dekker, C. *Nano Lett.* **2008**, *8* (2), 685–688.
- (10) Heller, I.; Chatoor, S.; Mannik, J.; Zevenbergen, M. A. G.; Oostinga, J. B.; Morpurgo, A. F.; Dekker, C.; Lemay, S. G. *Nano Lett.* **2010**, *10* (5), 1563–1567.
- (11) Peng, H. B.; Hughes, M. E.; Golovchenko, J. A. *Appl. Phys. Lett.* **2006**, *89* (24), No. 243502.

- (12) Chan, J.; Burke, B.; Evans, K.; Williams, K. A.; Vasudevan, S.; Liu, M. G.; Campbell, J.; Ghosh, A. W. *Phys. Rev. B* **2009**, *80* (3), No. 033402.
- (13) Liu, F.; Bao, M. Q.; Kim, H. J.; Wang, K. L.; Li, C.; Liu, X. L.; Zhou, C. W. *Appl. Phys. Lett.* **2005**, *86* (16), No. 163102.
- (14) Liu, F.; Wang, K. L.; Li, C.; Zhou, C. W. *IEEE Trans. Nanotechnol.* **2006**, *5* (5), 441–445.
- (15) Liu, F.; Bao, M. Q.; Wang, K. L. *Nano Lett.* **2005**, *5* (7), 1333–1336.
- (16) Liu, F.; Wang, K. L. *Nano Lett.* **2008**, *8* (1), 147–151.
- (17) Liu, F.; Bao, M. Q.; Wang, K. L.; Zhang, D. H.; Zhou, C. W. *Phys. Rev. B* **2006**, *74* (3), No. 035438.
- (18) Kamimura, T.; Hayashi, H.; Matsumoto, K. Physical and Chemical Properties of Carbon Nanotubes. In *Control of Single-Hole Transition in Carbon Nanotube Transistor with Quantum Dot in Gate Insulator at Room Temperature*; Suzuki, S., Ed.; InTech: Rijeka, Croatia, 2013.
- (19) Ralls, K. S.; Skocpol, W. J.; Jackel, L. D.; Howard, R. E.; Fetter, L. A.; Epworth, R. W.; Tennant, D. M. *Phys. Rev. Lett.* **1984**, *52* (3), 228–231.
- (20) Wang, N. P.; Heinze, S.; Tersoff, J. *Nano Lett.* **2007**, *7* (4), 910–913.
- (21) Kong, J.; LeRoy, B. J.; Lemay, S. G.; Dekker, C. *Appl. Phys. Lett.* **2005**, *86* (11), No. 112106.
- (22) Sharf, T.; Kevek, J. W.; DeBorde, T.; Wardini, J. L.; Minot, E. D. *Nano Lett.* **2012**, *12* (12), 6380–6384.
- (23) Minot, E. D.; Janssens, A. M.; Heller, I.; Heering, H. A.; Dekker, C.; Lemay, S. G. *Appl. Phys. Lett.* **2007**, *91*, (9).
- (24) Kittel, C. *Introduction to Solid State Physics*; John Wiley & Sons, Inc.: New York, 2005.
- (25) Purewal, M. S.; Hong, B. H.; Ravi, A.; Chandra, B.; Hone, J.; Kim, P. *Phys. Rev. Lett.* **2007**, *98* (18), No. 186608.